

Electronic Supplementary Information

Surface Fibrillation of Para-aramid Nonwoven as a Multi-functional Air Filter with Ultralow Pressure Drop

*Kangli Xu^a, Jixia Deng^a, Rui Lin^b, Heng Zhang^c, Qinfei Ke^{*a}, and Chen Huang^{*a}*

^aKey Laboratory of Textile Science & Technology, Ministry of Education, College of Textiles, Donghua University, Shanghai 201620, China.

^bLaboratory of Clean Energy Utilization and Pollution Control, College of Environmental Science and Engineering, Donghua University, Shanghai 201620, China.

^cState Key Lab High Performance Ceram & Superfine, Shanghai Institute of Ceramics, Chinese Academy of Sciences, Shanghai 200050, China.

Synthesis of ball-like CeO₂

0.25 g Ce(NO₃)₃·6H₂O was added into the mixed solution containing 0.6 mL deionized water, 0.4 mL acetic acid and 15 mL ethanol. The above solution was stirred at room temperature for 30 min and transferred to a 50 mL Teflon-line stainless steel autoclave reactor and reacted at 180 °C for 24 h. When the autoclave was cooled to room temperature, the product was washed by water and ethanol three times each in a centrifuge. The obtained catalyst was dried overnight in an oven at 60 °C, and then calcined in a muffle oven at 500 °C for 2 h.

Synthesis of rod-like CeO₂

0.4 g Ce(NO₃)₃·6H₂O and 3.367 g NaOH were dissolved in 5 mL and 35 mL deionized water, respectively. The above solutions were mixed and stirred at room temperature for 30 min, and then transferred to a 100 mL Teflon-line stainless steel autoclave reactor and reacted at 100 °C for 24 h. When the autoclave was cooled to room temperature, the product was washed with water and ethanol three times each with a centrifuge. The obtained catalyst was dried overnight in an oven at 60 °C, and then calcined in a muffle oven at 500 °C for 2 h.

Synthesis of flower-like CeO₂

1 g CTAB was dissolved in 100 mL deionized water, 4.34 g $\text{Ce}(\text{NO}_3)_3 \cdot 6\text{H}_2\text{O}$ was added to the solution, and was stirred at room temperature for 2 h until it was completely dissolved to form a transparent solution. 7.727 mL ammonia was dissolved in 50 mL water, and added to the above solution at the rate of 30 rpm, adjusting the PH value to about 10. The reaction was stirred at room temperature for 1 h. Then the solution was transferred to a 100 mL Teflon-line stainless steel autoclave reactor and reacted at 160 °C for 24 h. When the autoclave was cooled to room temperature, the product was washed with water and ethanol three times each with a centrifuge. The obtained catalyst was dried overnight in an oven at 60 °C, and then calcined in a muffle oven at 500 °C for 2 h.

Synthesis of CuO

1.21 g $\text{Cu}(\text{NO}_3)_2 \cdot 3\text{H}_2\text{O}$ and 4.0 g NaOH were dissolved in 50 mL deionized water respectively. The above solutions were mixed and stirred at 50 °C for 2 h, and the product was washed *via* deionized water and ethanol three times each with a centrifuge. The obtained particles were dried under vacuum at 60 °C for 12 h, and then calcined at 500 °C for 2 h in air.

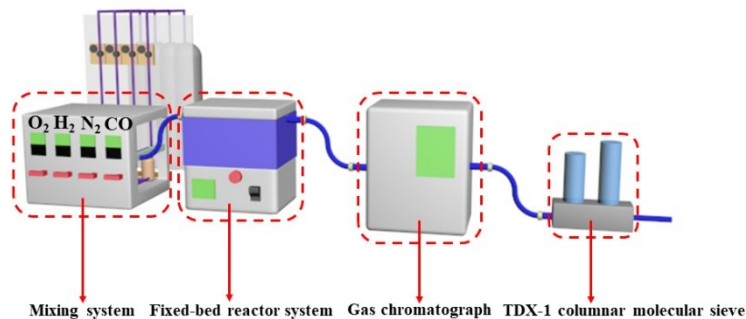


Figure S1. Device schematic diagram of CO conversion testing.

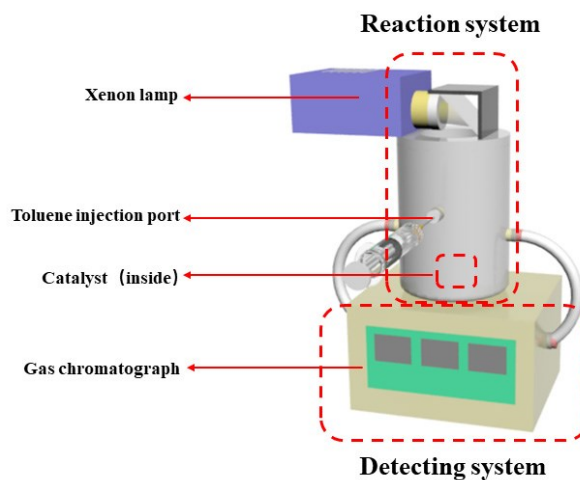


Figure S2. Device schematic diagram of toluene catalytic testing.

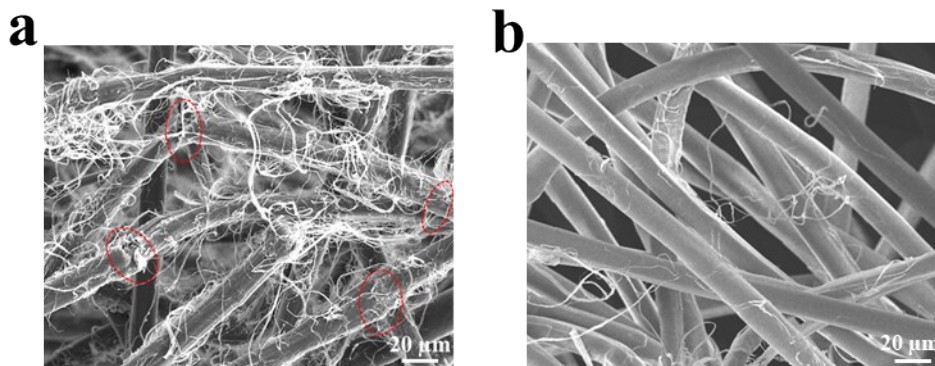


Figure S3. SEM images of para-aramid nonwovens fibrillated by (a) sulfuric acid (H_2SO_4) and (b) acetic acid (CH_3COOH), respectively.

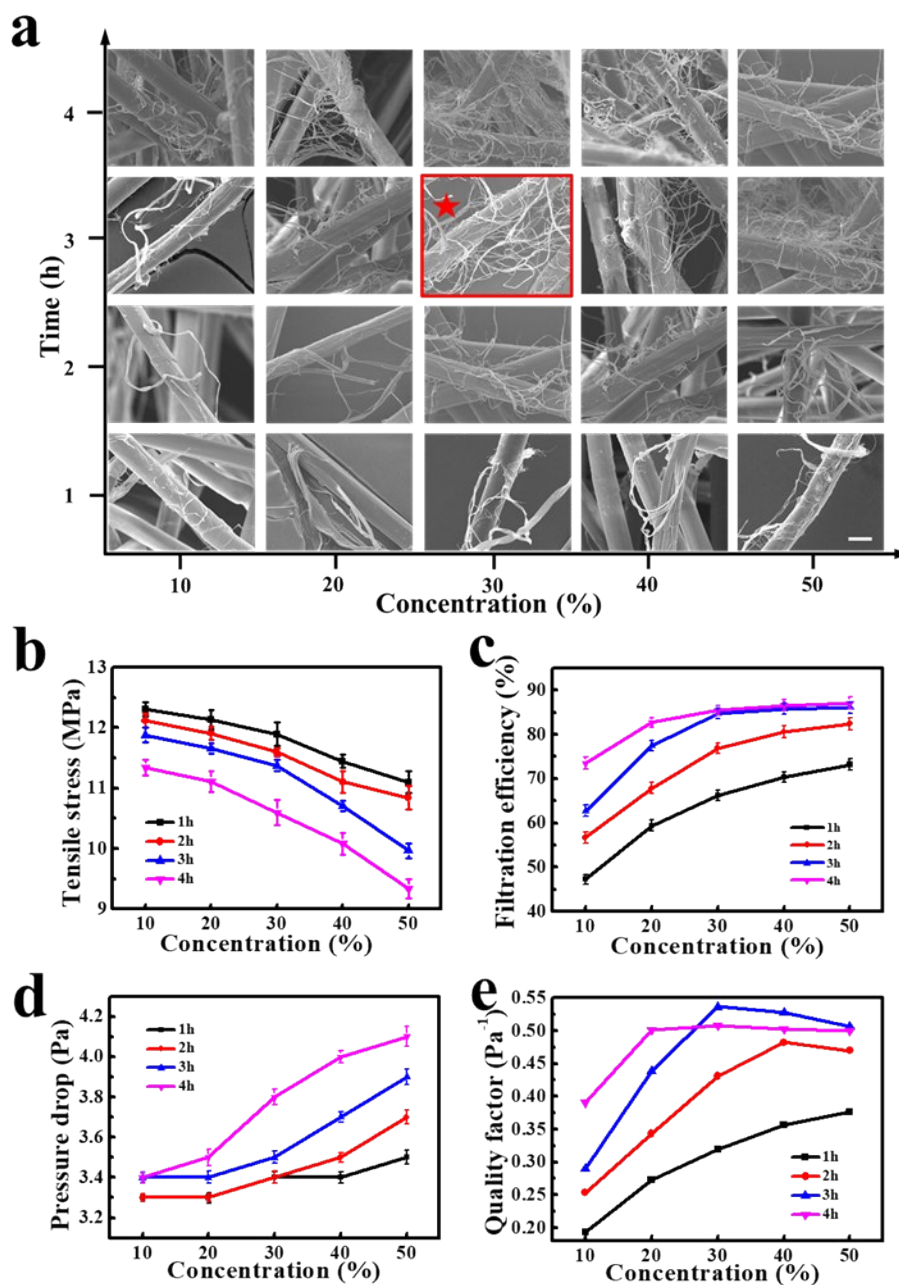


Figure S4. (a) SEM images, (b) tensile stress, (c) filtration efficiency, (d) pressure drop and (e) quality factor of para-aramid nonwovens treated in different concentrations of H_3PO_4 solution at different time. The optimal sample is pointed out by the red star. Scale bar = 20 μm .

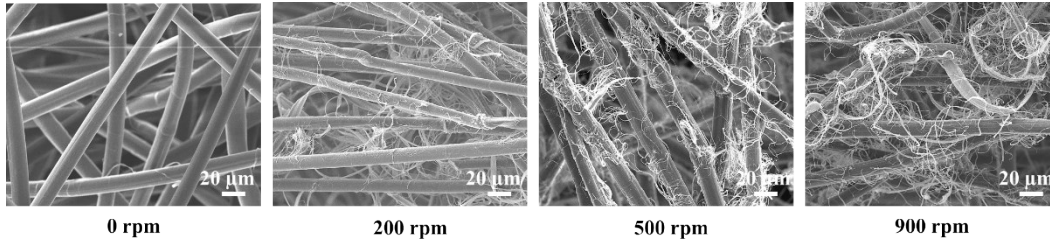


Figure S5. SEM images of para-aramid nonwovens fibrillated in H_3PO_4 solution by different stirring speeds.

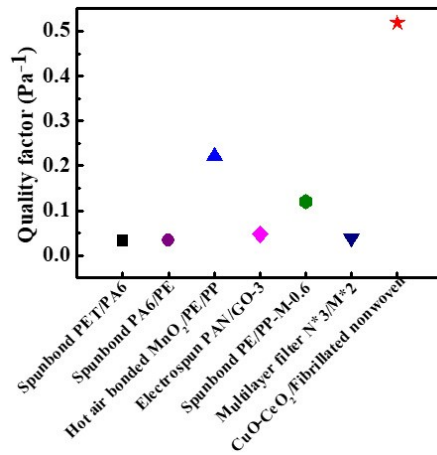


Figure S6. Filtration performance of selected materials for air filtration.

The quality factor (QF) was calculated by the following formula:

$$QF = -\ln(1-\eta) / \Delta p \quad (1)$$

where η and Δp represent the average filtration efficiency and the average pressure drop, respectively.

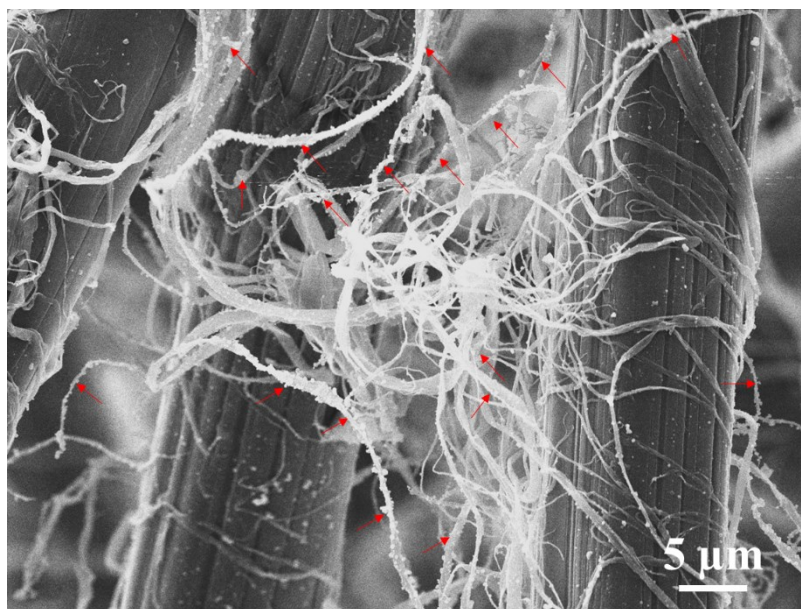


Figure S7. Deposition of NaCl particles on the fiber surface after filtration. The particles on nanofibers are denoted by red arrows.

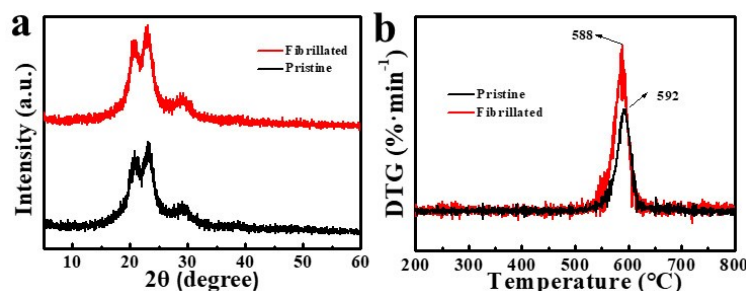


Figure S8. (a) XRD and (b) DTG curves of pristine and fibrillated nonwovens.

X-ray diffraction pattern of para-aramid nonwovens before and after H_3PO_4 treatment is shown in Figure S8a. Both nonwovens have three peaks in the diffraction pattern, and the position of peaks has no obvious change. It shows that the conditions of H_3PO_4 treatment are relatively mild, and crystallinity of the nonwoven increases from 59.71% to 61.07% after fibrillation. This is because that hydrolysis and physical shearing majorly take place on the surface of para-aramid fiber, thus has little effects on crystallinity. Figure S8b are the thermal performance curves of para-aramid nonwovens before and after fibrillation. The mass loss of para-aramid nonwovens before 560 °C is relatively small, whereas further increase of temperature leads to a sharp decrease of mass. Derivative thermogravimetry (DTG) shows that the maximum weight loss rate of the fibrillated nonwoven is slightly higher than that of the pristine nonwoven, and the corresponding temperature is ~ 6 °C lower than that of the pristine nonwoven. This is probably because that the nanofibers on the surface of fibrillated para-aramid nonwoven are the first to lose weight due to the low molecular weight. In general, thermal stability of para-aramid nonwoven treated by H_3PO_4 solution maintains at a high level.

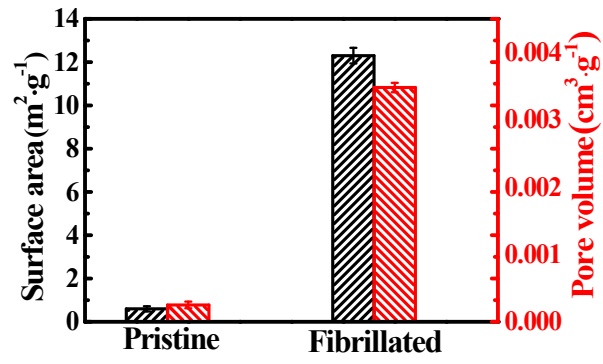


Figure S9. Surface area and pore volume of para-aramid nonwovens before and after fibrillation.

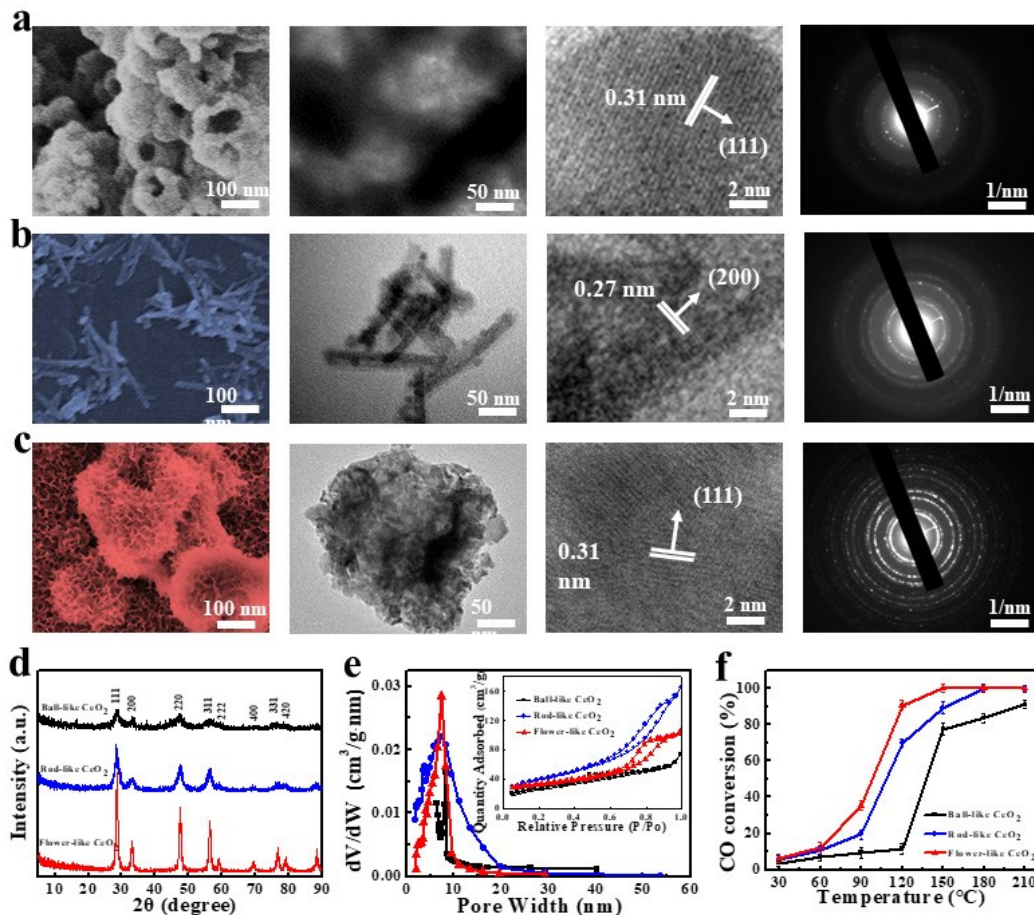


Figure S10. SEM images, TEM images, corresponding HRTEM images and electron diffraction patterns of (a) ball-like CeO₂, (b) rod-like CeO₂ and (c) flower-like CeO₂. (d) XRD patterns, (e) pore size distribution calculated from the BJH desorption branch, (inset is the N₂ adsorption-desorption isotherms), and (f) CO oxidation of CeO₂ catalysts with different morphologies.

The activity of CeO₂-based catalysts depends largely on the activity of CeO₂^{S1}. Therefore, we preliminarily regulated the morphology of CeO₂ and compared its effect on the degradation of CO. Figure S10a-c are the CeO₂ particles with ball-like, rod-like and flower-like features. It can be seen from SEM and TEM images that the sizes of ball-like and flower-like particles are ~150 nm and ~250 nm, respectively, while rod-like particles are ~180 nm in length and 30 nm in width. The reflections with interplanar crystal spacings of 0.27 nm and 0.31 nm in their corresponding

HRTEM images are assigned to CeO₂ planes (200) and (111), and the polycrystalline surface of CeO₂ is proved by the diffraction rings in SAED patterns. The purity and crystallinity of three CeO₂ particles were compared by XRD (Figure S10d). All the characteristic peaks coincide well with those of the cubic phase of CeO₂ (JCPDS 34-0394), and no peaks of impurities were found. The flower-like CeO₂ exhibits the highest peak intensity, indicating a higher crystallinity than the ball-like and rod-like counterparts. N₂ adsorption-desorption isotherms and pore size analyses (Figure S10e) further prove the mesoporous structures of CeO₂ with different morphologies. The flower-like CeO₂ has the narrowest pore size distribution, and more than 99.12 % of its pores range from 2 to 20 nm. In consistency with previous work,^{S2} such a pore size range is associated with a larger surface area (Table S1), which is beneficial for the catalyst to expose more active sites^{S3}. Therefore, the flower-like CeO₂ presents the highest elimination rate of CO (Figure. S10f), and was selected for the following study.

Table S1. Textural properties of three different morphologies of CeO₂.

Sample	Surface area S _{BET} (m ² ·g ⁻¹)	Pore diameter D _p ^a (nm)	Pore volume V _p (cm ³ ·g ⁻¹)
Ball-like CeO ₂	106.79	5.95	0.16
Rod-like CeO ₂	68.86	7.83	0.13
Flower-like CeO ₂	139.18	7.34	0.26

Table S2. Textural properties of CuO-CeO₂ catalysts with different molar percentages of Cu.

Sample	Surface area S _{BET} (m ² ·g ⁻¹)	Pore diameter D _p ^a (nm)	Pore volume V _p (cm ³ ·g ⁻¹)	Molar content of Cu
0.05 CuO-CeO ₂	103.29	9.74	0.25	0.05
0.10 CuO-CeO ₂	91.35	16.21	0.37	0.10
0.15 CuO-CeO ₂	89.06	11.61	0.26	0.16

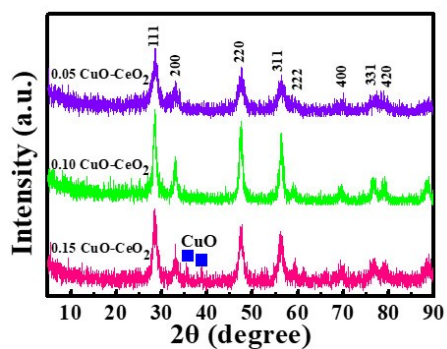


Figure S11. XRD patterns of 0.05 CuO-CeO₂, 0.10 CuO-CeO₂ and 0.15 CuO-CeO₂.

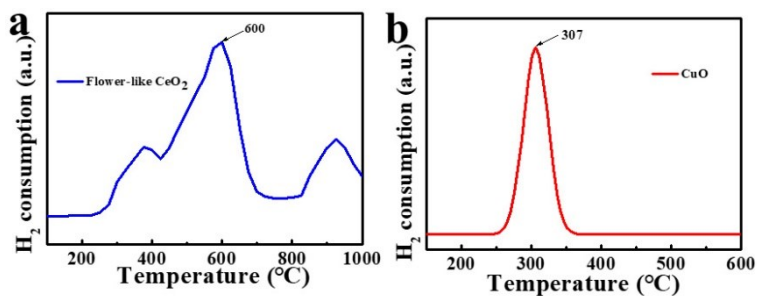


Figure S12. H₂-TPR profiles of (a) flower-like CeO₂ and (b) pure CuO.

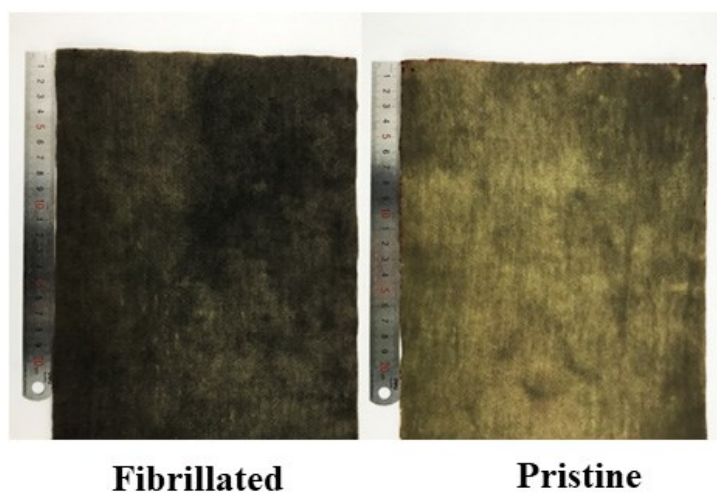


Figure S13. Digital photos of CuO-CeO₂ applied on fibrillated and pristine nonwovens.

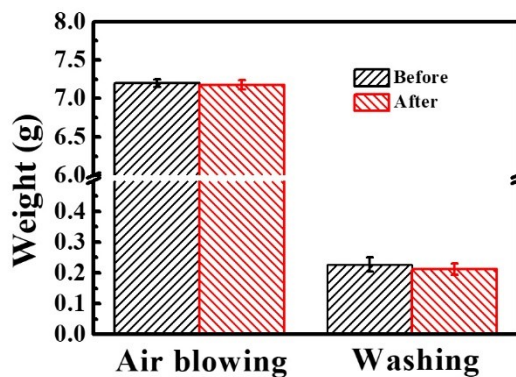


Figure S14. Weight changes of CuO-CeO₂/fibrillated nonwoven after repeated air blowing and washing for 3 times.

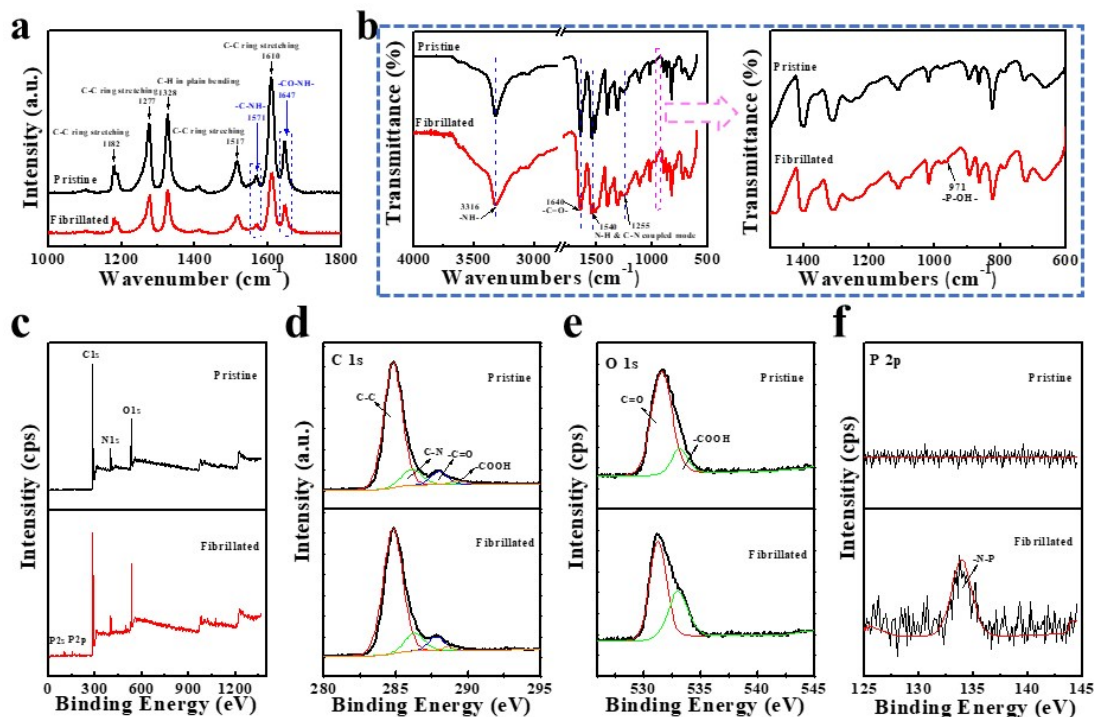


Figure S15. (a) Raman scattering, (b) FTIR spectrum, (c) wide-scan XPS spectra, (d) C1s, (e) O1s and (f) P2p spectra of pristine and fibrillated para-aramid nonwoven.

As shown in Figure S15a, the intensities of peaks at 1571 cm⁻¹ (C-N and N-H) and 1647 cm⁻¹ (C=O, C-N and N-H) are weakened by fibrillation, which is due to the cleavage of amide groups (-CONH-). The hydrolysis reaction of -CONH- produces carboxyl groups (-COOH) and amino groups (-NH₂), results in the enhanced stretching vibration of N-H bond at 3302 cm⁻¹ with the increase of -NH₂ (Figure S15b). In addition, the strong electron donating ability of -CONH- in

para-aramid molecular chain improves the reactivity of para and ortho hydrogen on the benzene ring. During H_3PO_4 treatment, a number of -OH are introduced into the benzene ring by electrophilic substitution. The introduction of -OH enhances the association of intermolecular hydrogen bonds and broadens the stretching vibration peak of hydrogen-bonded N-H group in the FTIR spectrum of fibrillated nonwovens. H_3PO_4 treatment also results in a clear absorption peak of -P-OH group at 971 cm^{-1} . The chemical bonds of the pristine and fibrillated para-aramid nonwoven were investigated via XPS analysis (Figure S15c-f). In the wide-scan XPS spectrum (Figure S15c), P2s and P2p photoelectron peaks were found in the fibrillated nonwovens, and the intensity of O1s photoelectron peak was enhanced, indicating the introduction of phosphorus and oxygen groups on the surface of para-aramid fibers. The C1s spectra of para-aramid nonwoven are fitted to four peaks with binding energies of 284.8, 286.1, 288.0 and 289.3 eV, which are attributed to C-C, C-N, C=O of amide groups, and -COOH, respectively. The presence of the -COOH groups in the C1s and O1s spectra (Figure S15d-e) indicates that a part of the amide groups in pristine fibers have already been hydrolyzed before H_3PO_4 treatment. However, the intensity of -COOH peaks increases obviously after the treatment. In Figure S15f, the binding energy at 133.7 eV shows P2p photoelectron peak (-N-P), which is formed by the covalent bonds between H_3PO_4 and -NH.

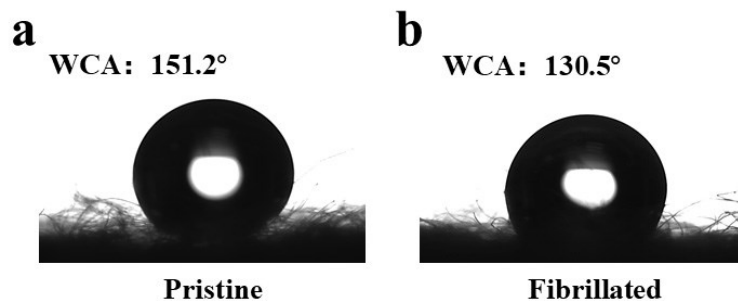


Figure S16. Water Contact angle (WCA) of (a) pristine and (b) fibrillated para-aramid nonwovens.

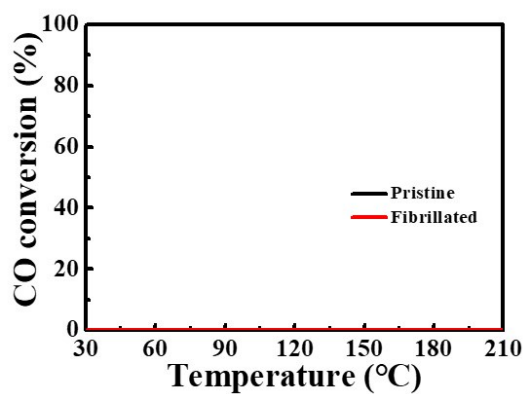


Figure S17. CO conversion of pristine and fibrillated para-aramid nonwovens.

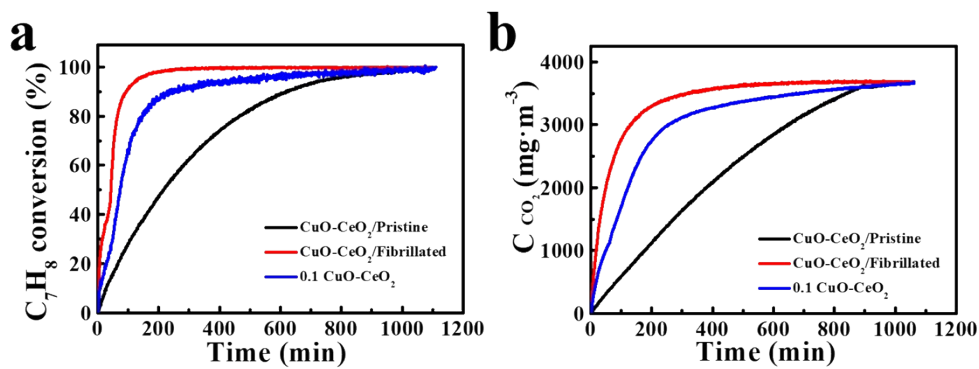


Figure S18. C₇H₈ catalytic performance of pristine and fibrillated para-aramid nonwovens loaded with CuO-CeO₂.



Figure S19. Digital photo of a large piece of CuO-CeO₂/fibrillated para-aramid nonwoven.

References

- 1 Y. Zeng, Y. Wang, F. Song, S. Zhang and Q. Zhong, *Sci. Total. Environ.*, 2020, **712**, 135635.
- 2 B. Zhang, Y. Huyan, J. Wang, W. Wang, Q. Zhang and H. Zhang, *J. Amer. Ceram. Soci.*, 2018.
- 3 P. Gong, J. Xie, D. Fang, X. Liu, F. He and F. Li, *Chem. Eng. J.*, 2019, **356**, 598-608.